Hindawi
Journal of Nanomaterials
Volume 2018, Article ID 9236450, 11 pages
https://doi.org/10.1155/2018/9236450

Research Article

Fast-LPG Sensors at Room Temperature by α-Fe_2O_3/CNT Nanocomposite Thin Films

B. Chaitongrat and S. Chaisitsak

Department of Electronics, Faculty of Engineering, King Mongkut's Institute of Technology Ladkrabang, Bangkok 10520, Thailand

Correspondence should be addressed to S. Chaisitsak; sutichai.ch@kmitl.ac.th

Received 24 November 2017; Accepted 11 January 2018; Published 14 February 2018

Academic Editor: Chengyuan Wang

We present performance of a room temperature LPG sensor based on α-Fe_2O_3/CNT (carbon nanotube) nanocomposite films. The nanocomposite film was fabricated via the metallic Fe catalyst particle on CNTs in which both the catalyst particles and the CNT were simultaneously synthesized by chemical vapor deposition (CVD) synthesis and were subsequently annealed in air to create α-Fe_2O_3. These methods are simple, inexpensive, and suitable for large-scale production. The structure, surface morphologies, and LPG response of nanocomposite films were investigated. Raman spectroscopy and XPS analysis showed the formation of α-Fe_2O_3 on small CNTs (SWNTs). Morphological analysis using FE-SEM and AFM revealed the formation of the porous surface along with roughness surface. Additionally, the sensing performance of α-Fe_2O_3/CNTs showed that it could detect LPG concentration at lower value than 25% of LEL with response/recovery time of less than 30 seconds at room temperature. These results suggest that the α-Fe_2O_3/CNTs films are challenging materials for monitoring LPG operating at room temperature.

1. Introduction

Liquefied petroleum gas (LPG) is a complex mixture of hydrocarbon compounds, which mostly consist of propane (C_3H_8) and butane (C_4H_{10}). LPG is widely used as a combustion apparatus in a heater, cooking equipment, and automotive vehicles. Besides, LPG is of most harmful gases due to its flammable, explosive nature, which presents many hazards to the human being as well as environment. To avoid the damage caused by leaks and gas explosions, there is prevailing need to detect LPG leakage at the lower explosive limit (~2.0 vol.% of LPG) [1]. In last few decades, metal oxide semiconducting (MOS) materials have been extensively used as an LPG sensor [2, 3]. However, the optimal sensing properties of them operated along with high temperature (300–500°C). In such case, a heater needs to be installed for the sensors to function, causing increased power consumption, complexity, and investment budgets. To overcome these limitations, the fabrication of a LPG sensor operable at room temperature has gained essence importance [4, 5].

Many reports are available on the development of the LPG sensors that operate at room temperature, the reduction of the MOS size [6, 7], and the mixing of MOS with metal nanoparticles [8] including the fabrication of heterojunctions [4, 9–11], which is one of the most strategies used. Due to the mixing of MOS and other materials, it formed a variety of the unique properties for sensing material, such as a change in conductance, improved surface catalytic property, increasing surface reaction sites, and producing a high porosity [12]. In addition, a formed contact potential at the interface between MOS and other nanostructured materials has also enhanced the sensing performance of a gas sensor [13, 14]. Therefore, more studies in fabricating devices based on heterojunctions are necessary, especially in nanostructure systems.

Iron oxide (Fe_2O_3) is n-type semiconductor, of which hematite (α-Fe_2O_3) is the most stable of Fe_2O_3. It has been widely studied for the various applications, including magnetic devices, pigments, catalysts, sensors, and medical fields [15]. In gas sensor applications, Fe_2O_3 has been continuously researched because it can provide high electron mobility, high chemical/thermal stability, multiple functions, and low cost [16, 17]. Recently, the nanostructures of Fe_2O_3 materials have attracted much attention as an effective material for various

gases because of their high surface activities, high surface-to-volume ratios, and high carrier mobility [18]. However, their electrical conductivity is limited, because it requires high temperatures to work [19]. Meanwhile, CNT can be considered as highly conductive material at room temperature. Additionally, CNTs have a hollow structure, nanosized morphology (diameter 1–10 nm), and high surface area (500–1500 m^2/g) [20–24]. Therefore, CNTs have been used for mixtures enhanced in the conductivity of Fe_2O_3 at room temperature [19, 25]. Moreover, Fe_2O_3 and CNTs nanocomposites have been fabricated through asynchronous methods, and then the mixture of Fe_2O_3 and CNT has been deposited on the substrate, usually using the usually spinning and screen-printing technique [25, 26]. However, these techniques are the major performance-limiting factors in the sensor because of its inhomogeneous film thickness. Therefore, the sensor fabrication process also provides the enhancement in sensing performance, which can control the porosity and the roughness, resulting in the improvement of sensing properties of the sensor. Recently, a new strategy to synthesize metal nanoparticle/CNT hybrid materials has been reported. Both of the Fe catalyst particles and the CNT are simultaneously synthesized. Then, the metallic Fe was transformed into maghemite (γ-Fe_2O_3) nanoparticles via a potential-cycling method [27].

Here, we report an effective approach to fabricate the α-Fe_2O_3/CNT nanocomposite films, in which the CNT was uniformly coated with α-Fe_2O_3 particles (α-Fe_2O_3/CNTs). According to our previous work [28], we found that the Fe catalyst particles adhere to as-grown CNTs. In this work, those particles were annealed in air to create α-Fe_2O_3 into CNTs films. In addition, we also demonstrate the application of the α-Fe_2O_3/CNTs thin films as a LPG sensor. Obtained results indicated that the response and recovery time of sensor have been significantly improved for detecting LPG at room temperature (28°C). Moreover, the sensing mechanisms of α-Fe_2O_3/CNTs-based LPG sensor were also discussed.

2. Experimental Section

2.1. Fabrication of α-Fe_2O_3/CNT Thin Films. An α-Fe_2O_3/CNTs films-based sensor was fabricated through the following processes. Firstly, as-grown CNTs were synthesized through the vertical floating catalyst chemical vapor deposition method (FC-CVD) using pyrolysing solutions of ethanol-ferrocene. The details of synthesized as-grown CNTs have been previously reported [28]. Briefly, a precursor was prepared by dissolving ferrocene powder (Fe $(C_5H_5)_2$; Sigma-Aldrich) in ethanol solution (C_2H_5OH; Carlo Erba) at a 0.25 wt.% ferrocene/ethanol ratio. The mist of precursor solution was carried into the 960°C reactor via argon (Ar) gas with a flow rate of 1000 sccm. The synthesized CNTs were collected onto a membrane filter directly from the FC-CVD reactor at the bottom of the reactor under room temperature (hereinafter called "as-grown CNTs"). The density of as-grown CNTs was controlled by adjusting deposition time (study; 15, 30, 45, 60, 90, and 120 min). Secondly, as-grown CNT films were then transferred from the filter to a slide glass or silicon (Si) substrate by pressing and then dissolving the filter in acetone. Finally, the as-grown CNTs on substrate were put into a laboratory oven and annealed in air atmosphere at 350°C for 8 h to create α-Fe_2O_3 (hereinafter "α-Fe_2O_3/CNTs"). In order to investigate the effect of standalone CNTs on the gas sensing properties, α-Fe_2O_3/CNTs films were purified by immersing in 3 M hydrochloric acid (HCl) to remove α-Fe_2O_3, resulting in a purified CNTs film (hereinafter called "purified CNTs").

2.2. Characterizations. The characteristics of CNTs were analyzed by Raman spectroscopy (Renishaw inVia Reflex) with an Ar laser (514.5 nm) as the excitation source. The surface composition changes of as-grown and α-Fe_2O_3/CNTs were measured by X-ray photoelectron spectroscopy (XPS; PHI 5700), which were carried out on an AXIS Ultra DLD-X-ray photoelectron spectrometer using a monochromatic Al K_α source (1486.6 eV). In order to analyze the chemical functional group of the samples, the Fe 2p, O 1s, and C 1s core level were deconvoluted using the Shirley background function and Vigt fit. The surface morphology of films was performed by field-emission scanning electron microscopy (FE-SEM: JEOL, Hitachi s4700), atomic force microscopy (AFM: Park Systems XE100), and transmission electron microscopy (TEM: JEOL, JSM-2010). The sensor was placed into the chamber; N_2 (or zero air) and LPG were then injected via a mass flow controller unit (MFC). The gas sensing characteristics of the sensor were examined by monitoring changes in resistance with a constant voltage of 5 V, using Keithley source meter (Model 2004). Data acquisitions (DAQ), storage, and plotting in real time were realized using a personal computer with LabView™ software via a GPIB interface control.

3. Results and Discussion

3.1. Raman Spectroscopy Analyses. Figure 1(a) presents the Raman spectra of the as-grown CNT and α-Fe_2O_3/CNT nanocomposite films in the low-frequency (~100–500 cm^{-1}) region. The as-grown CNT films show several characteristic peaks at 162 and 267 cm^{-1}. These peaks are the Raman spectra in radial breathing mode (RBM: ~100–350 cm^{-1}) of the small-diameter CNTs (SWNTs: single-walled CNTs), which corresponded to the diameters (Φ_{SWNTs}) of the CNTs films varying in the range of 0.9–1.5 nm [29]. It is clearly seen from this figure that CNTs with 1.5 mm diameter remain after the anneal, while the small tube (0.9 nm) is easily burned at 350°C due to curvature strain [30]. In addition, Raman spectra of α-Fe_2O_3/CNT nanocomposite films also reveal additional peaks at 227, 244, 298, and 414 cm^{-1} but these peaks are small signals (see inset of Figure 1(a)). These peaks remained after removing CNTs by annealing at 550°C, which can clearly observe the main peak at 298 cm^{-1}, 414 cm^{-1}, and 1320 cm^{-1} and minor peaks at 227 cm^{-1} and 244 cm^{-1}. These peaks are identified to the hematite (α-Fe_2O_3) nanostructure [31, 32].

Figure 1(b) presents the Raman spectra of the as-grown CNT and α-Fe_2O_3/CNT nanocomposite films in the high-frequency (~1200–1800 cm^{-1}). In the high-frequency regions,

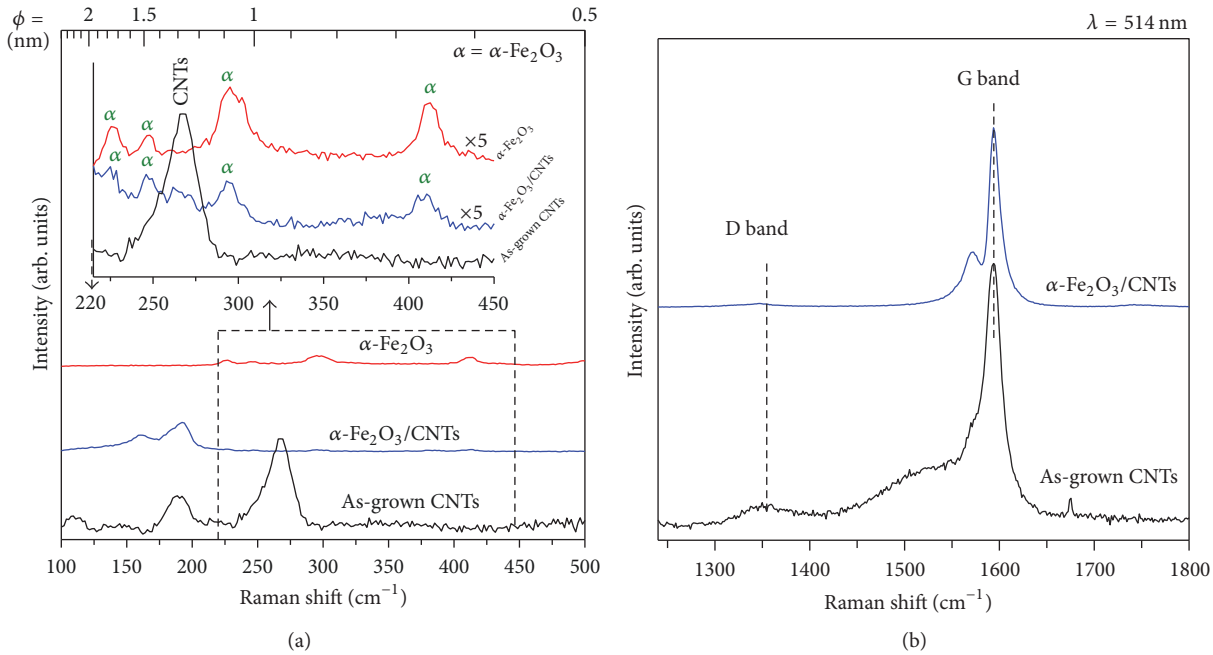

FIGURE 1: The Raman spectrum of the as-grown CNT and α-Fe_2O_3/CNT nanocomposite films measured in (a) low-frequency and (b) high-frequency regions. The inset in (a) shows a comparison between Raman spectra of as-grown CNTs, α-Fe_2O_3/CNTs, and α-Fe_2O_3 reference.

two apparent peaks at 1570 cm^{-1} and 1590 cm^{-1} are observed and correspond to the D and G band of CNTs [29]. The intensity ratio of G and D mode (I_G/I_D): a higher ratio indicates a lower defect, therefore, better structural quality [29]. I_G/I_D of as-grown CNT and α-Fe_2O_3/CNTs are 11.9 and 12.3, respectively. It can be seen that I_G/I_D of α-Fe_2O_3/CNT films had higher than that of as-grown CNT films. I_G/I_D results indicated that the purity of CNTs increased and the structure of CNTs was not damaged even when annealed in air.

3.2. XPS Analyses. The XPS technique is used to analyze chemical composition on the top surface of the materials (depth < 10 nm). Compositional elements can be identified by the peak position in terms of binding energy and the peak intensity (peak area) can be related to the amount of elements in the material.

Figure 2(a) demonstrates that the XPS survey spectrum of both as-grown CNTs and α-Fe_2O_3/CNT films was carbon (C 1s; ~284 eV), oxygen (O 1s; ~530 eV), silicon (Si 2p; ~100 eV), silver (Ag 3d; ~370 eV), and iron (Fe 2p; ~700 eV) [33–35]. In α-Fe_2O_3/CNT thin films, peak at 100 eV is observed and corresponds to silicon of silicon substrate; this is because of the ultra-thin films of the Fe_2O_3/CNTs. In addition, the atomic percent (At%) table (see the inset table) demonstrated that the O : Fe atomic ratio on the α-Fe_2O_3/CNT films was close to 2 : 3, which is probably Fe_2O_3 [25].

The phase analyses in α-Fe_2O_3 have been achieved via the Fe 2p deconvolution, as shown in Figure 2(b). The peaks in the Fe 2p spectrum were considered as species of Fe in films, which is referenced in the previous reports of Fe_2O_3 [36–38]. Fe $2p_{1/2}$ and Fe $2p_{3/2}$ are doublet spin orbit component of Fe 2p. According to Figure 2(b), the as-grown CNT films were composed mostly of Fe metal, followed by Fe_3C (Fe-C), FeO, Fe_3O_4, and Fe_2O_3, respectively. After annealing, the dominant component in α-Fe_2O_3/CNT films was Fe_2O_3. In addition, two distinct peaks are observed at binding energies of 711.4 (Fe $2p_{3/2}$) and 724.4 (Fe $2p_{1/2}$) eV with a broad shake-up-satellite peaking at 719.3 eV. These peaks suggested that the phase formation of α-Fe_2O_3 was as good as those reported in the previous α-Fe_2O_3 studies [18, 36]. The occurrence of α-Fe_2O_3 is similar to that obtained by our Raman results. These results indicated that the most of Fe elements in α-Fe_2O_3/CNT films were α-Fe_2O_3, followed by the Fe_3O_4, Fe $(OH)_x$, and Fe-Si, respectively. The increase in intensity of the O 1s deconvoluted peak at 530.4 eV indicated that the surface of α-Fe_2O_3 had mostly adsorbed oxygen ions [39], as shown in Figure 2(c). The peaks at 532.4, 533.4, and 534.2 eV corresponded to carboxylate/carbonyl (O–C=O/C=O), epoxy/hydroxyl (C–O–C/C–OH), and silicon oxide (Si–O) respectively. It should be noted that the α-Fe_2O_3/CNTs showed the occurrence of a new peak at 531.7 eV (in O 1s deconvolution; Figure 2(c)) and that Fe–C (in Fe 2p deconvolution; Figure 2(b)) disappeared. This may be that bonding of metallic Fe and CNTs (Fe–C) was changed to α-Fe_2O_3 and CNTs (Fe–O–C), of which Fe atom and CNTs were contacted via carbonyl groups (–O–C). The peak at 531.7 eV, therefore, possibly is assigned to the binding of α-Fe_2O_3 and oxygen functional group on CNTs through Fe–O–C bonds.

Furthermore, more structure and characterization of the CNTs were carried out by the C 1s deconvolution [39], as shown in Figure 2(d). Both of as-grown CNT and α-Fe_2O_3/CNT films presented the main peak at 284.9 eV, which can be assigned the C 1s (Sp^2) binding energy of CNTs. The

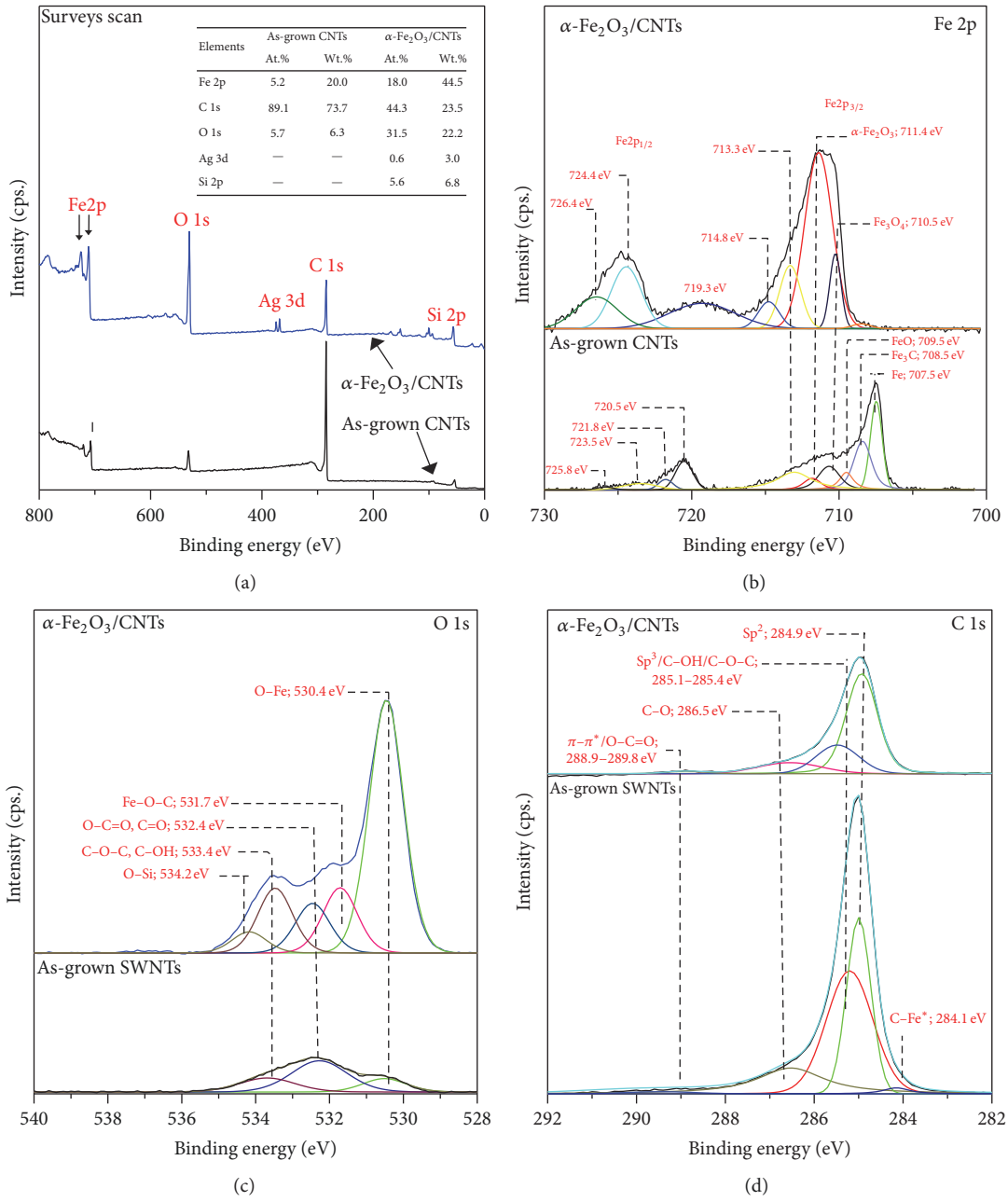

FIGURE 2: (a) XPS survey scan of as-grown CNTs and α-Fe_2O_3/CNT films. (b) XPS deconvolution of (b) Fe 2p, (c) O 1s, and (d) C 1s. The inset in (a) shows the atomic percent (At%) and weight percent (Wt%) of as-grown CNTs and α-Fe_2O_3/CNT films.

peaks in the shoulder of the main peak at 285.1–285.4, 286.5, and 288.9–289.8 eV could be assigned to Sp^3/C–OH/C–O–C, C–O, and π–π^*/O–C=O, respectively. Sp^3 was attributed to amorphous carbon/defects in the nanotube structure, which, at this defect, could be grafted to the –OH and –C–O [40, 41]. It is widely recognized that the mixing of oxide NPs by the formation of nucleus Fe^+ on CNTs induces damage in CNTs [25]. However, our method did not further significantly affect the CNTs due to the Fe spontaneously grow and uniformly assemble on the entire surface of each nanotube by CVD. In addition, the sp^2/sp^3 ratio of the α-Fe_2O_3/CNT films was higher than that of the as-grown CNT films. This is consistent with I_G/I_D ratios in the Raman results, implying that the structure of CNTs was not damaged even when annealed in air.

3.3. FE-SEM/AFM Analyses. From the obtained results from XPS and Raman spectroscopy, it is confirmed that the as-grown CNTs were decorated with metallic Fe. However, these metallic Fe could be easily transformed to α-Fe_2O_3 by air annealing. In this section, we investigated that the

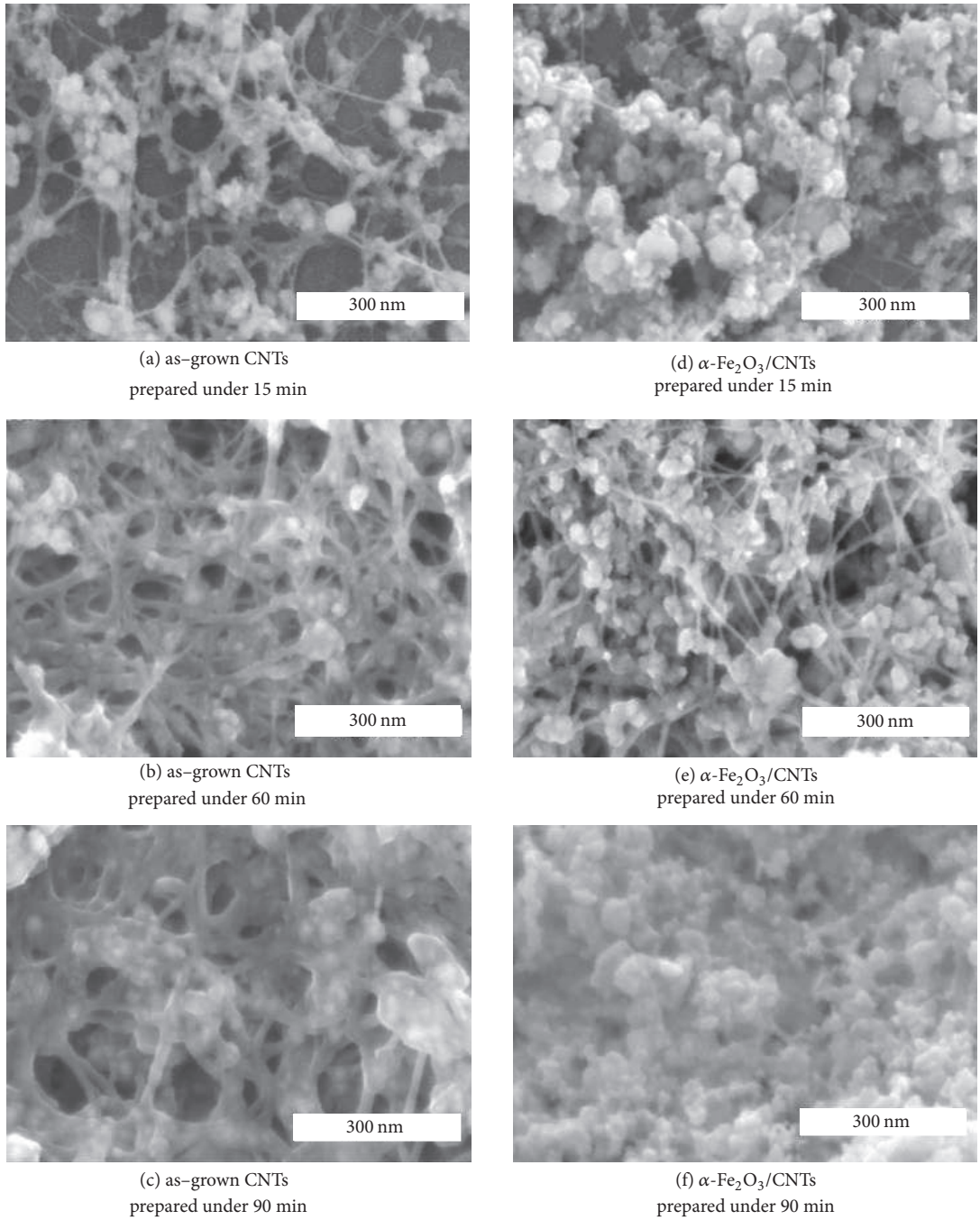

(a) as–grown CNTs prepared under 15 min

(d) α-Fe_2O_3/CNTs prepared under 15 min

(b) as–grown CNTs prepared under 60 min

(e) α-Fe_2O_3/CNTs prepared under 60 min

(c) as–grown CNTs prepared under 90 min

(f) α-Fe_2O_3/CNTs prepared under 90 min

Figure 3: Morphology of (a–c) as-grown CNT films and (d–f) α-Fe_2O_3/CNT composite films on glass substrate.

variation of deposition time effected on the morphology of α-Fe_2O_3/CNTs.

Figures 3(a)–3(c) present the SEM images of as-grown CNT films on silicon substrates, which were prepared at different deposition times of 15, 60, and 90 min, respectively. As-grown CNT films consist of CNTs and metallic Fe particles. The decrease in the distribution of CNTs and Fe particles suggest that the density of CNTs and Fe particles increases with increasing the deposition time. In addition, the hydroxide (OH–) part was observed onto CNTs and Fe particles in XPS result. These components may be attributed to the remained filters. The CNTs were the loosely packed and were consisted of the randomly oriented entangled CNT bundles, which were decorated with Fe NPs (size averaged 7.33 nm in diameter; Supplement Figure S1).

Figures 3(d), 3(e), and 3(f) present the SEM images of α-Fe_2O_3/CNT films prepared with different deposition time of 15, 60, and 90 min, respectively. The hydroxide part was removed during air annealing leading to the formation of α-Fe_2O_3 nanoparticles. It is seen that the CNTs network with

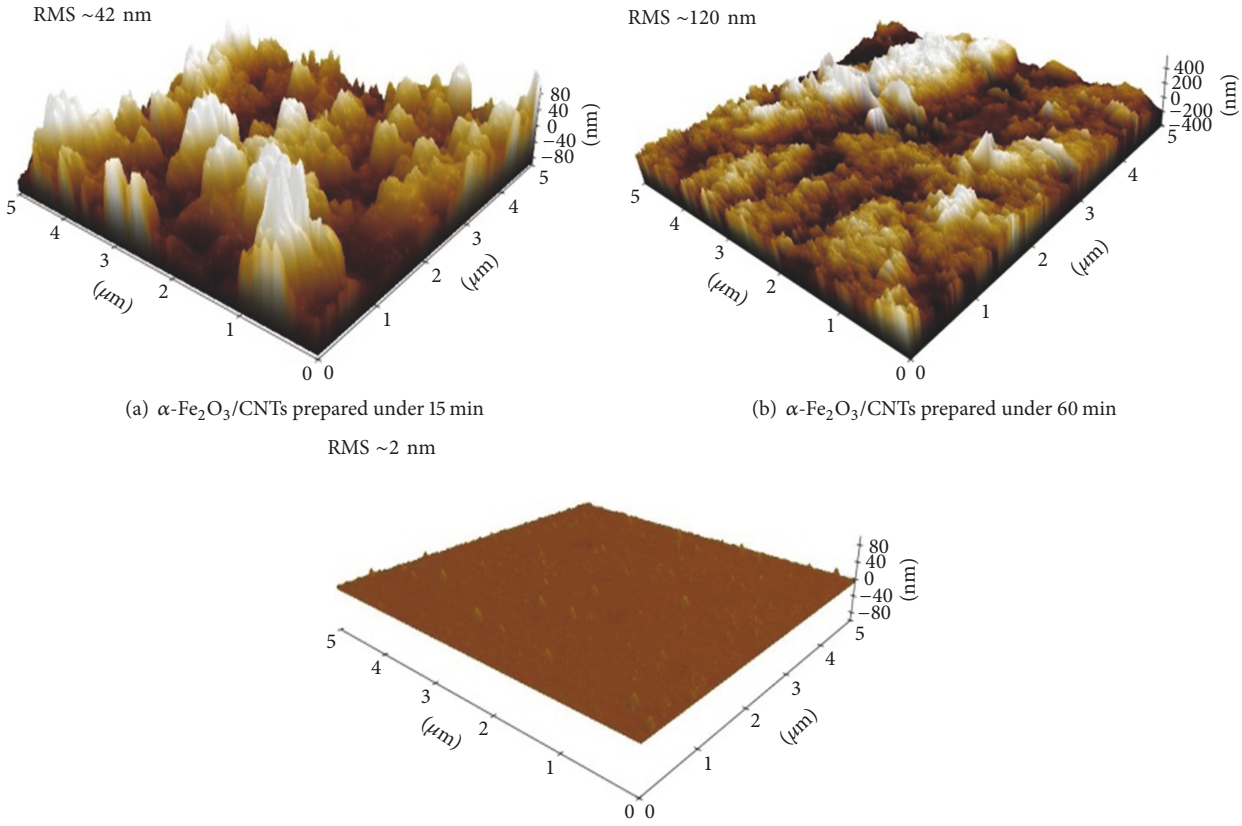

(a) α-Fe_2O_3/CNTs prepared under 15 min

(b) α-Fe_2O_3/CNTs prepared under 60 min

(c) α-Fe_2O_3/CNTs prepared under 90 min

FIGURE 4: Morphology of surface measured using AFM on samples of the α-Fe_2O_3/CNT films with different deposition times. The 3D images recorded at 5 μm × 5 μm planar in contact mode.

interconnected α-Fe_2O_3 nanoparticles is formed in Figures 3(d) and 3(e). In addition, the small agglomeration of the α-Fe_2O_3 particles is also observed at the interconnections of network structure along leading to the formation of the high porous surface. The α-Fe_2O_3/CNT structure with high porous is beneficial towards LPG sensing application because of the gas molecules enable to enter quickly through the porous structure.

Figures 4(a), 4(b), and 4(c) present that the AFM images of α-Fe_2O_3/CNT films. Root mean square (RMS) roughness of α-Fe_2O_3/CNT films is ~42, ~120, and ~2 nm for α-Fe_2O_3/CNT films prepared under deposition time of 15, 60, and 90 min, respectively. In our previous report [47], the sensor response of LPG sensor increases as a result of the high RMS value, because of the increase in the number of the active adsorption sites for oxygen or hydrocarbon molecules on the sensor surfaces.

According to SEM and AFM observations, it is seen that the porous structure and the surface roughness of α-Fe_2O_3/CNT films were controlled by deposition time along with spatial distribution of CNTs and α-Fe_2O_3 particles. SEM and AFM images (Figures 3(f) and 4(a)) of such α-Fe_2O_3/CNT films prepared under deposition time of 90 min clearly indicate that their surface had a bulk structure and low roughness. For a spatial distribution of Fe_2O_3/CNT films under prepared 90 min, small particles were closed together and easily aggregated into a flat surface with reduced surface area of α-Fe_2O_3/CNT films. Obtained results indicated that choosing a suitable deposition time could generate α-Fe_2O_3/CNT films along with a highly porous structure and high roughness.

3.4. Sensing Properties of LPG Sensors. The sensor response to LPG was defined as $S(\%) = (|\Delta R|/R_g) \times 100\%$, ΔR is $R_a - R_g$, where R_g and R_b denote the resistance of sensor when exposed to LPG gas and that when exposed to baseline gas, respectively [48]. Response/recovery time [49] is an important sensing performance indicator for a sensor to detect a flammable gas. A sensor's response time (T_{resp}.) is defined as 90% change in resistance from its baseline value to the maximum value in the presence of LPG. Recovery time (T_{rec}.) is defined as the time required for recovering of the original resistance. In the examination of the sensor, carbon conductive electrodes were added onto the top of sensing films.

Figures 5(a), 5(b), and 5(c) display the change in the resistance of as-grown CNTs, α-Fe_2O_3/CNTs, and purified CNTs sensors in the presence of LPG at various concentrations. The baseline resistances in N_2 for as-grown CNTs, α-Fe_2O_3/CNTs, and purified CNTs were approximately 2.5 kΩ, 1.9 MΩ, and 360 kΩ, respectively. Figure 5(a) presents that

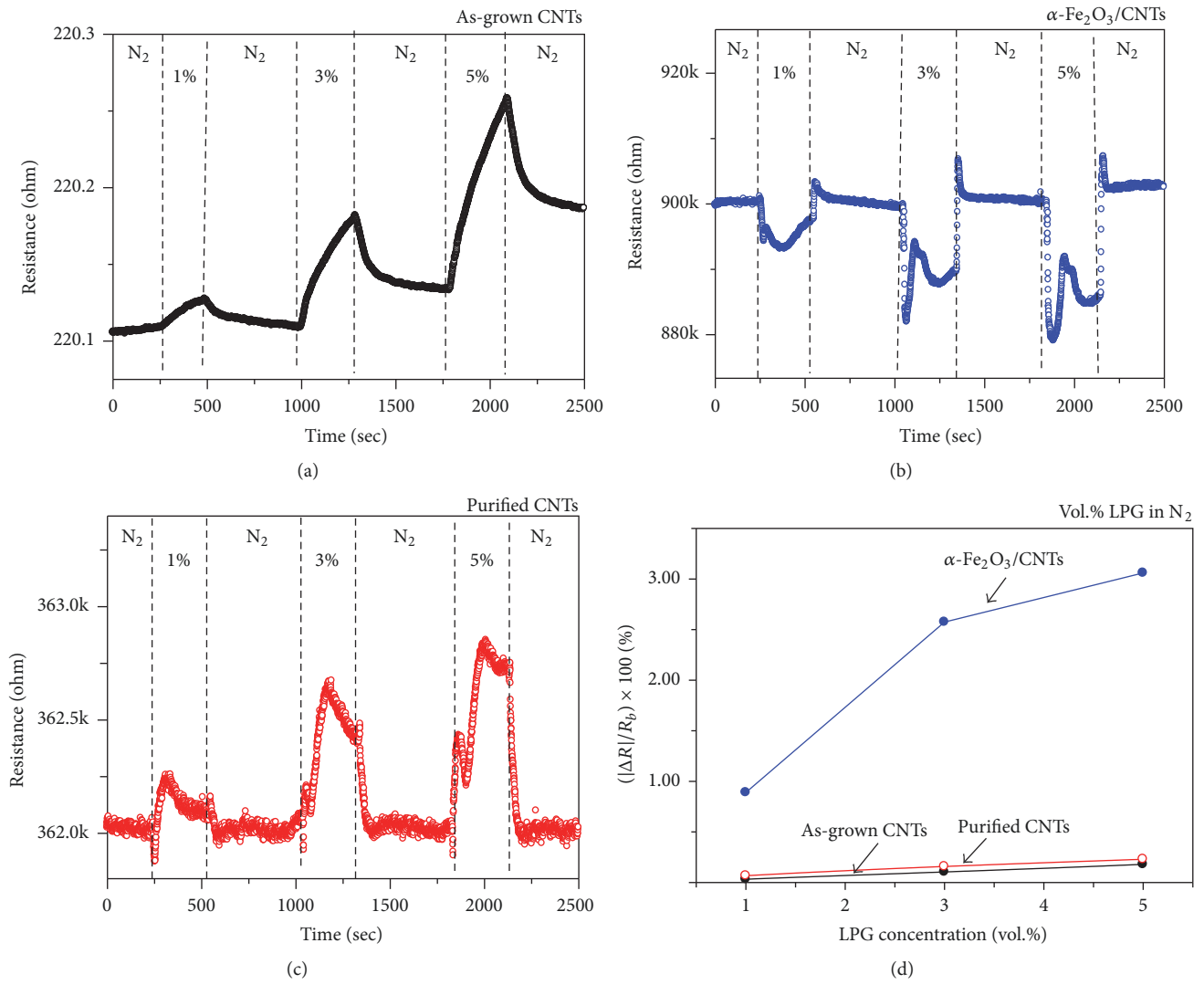

FIGURE 5: Dynamic responses of (a) as-grown CNTs; (b) α-Fe_2O_3/CNTs; and (c) purified CNTs to LPG in air atmosphere. (d) demonstrates sensor responses by sensor type to varying LPG concentrations of 1–5 vol.%.

the p-type LPG sensing behavior is observed for as-grown CNTs, which resulted from the CNTs sensing while the Fe catalyst was encapsulated with carbon [27]. Meanwhile, α-Fe_2O_3/CNT films display an n-type sensing behavior due to the formations of α-Fe_2O_3 that act as LPG sensing. It is well known that the sensing behavior of gas sensor has been related to the properties of sensing materials such as p-type material, which had hole majority carriers. The amount of hole will be decreased dramatically when reducing gas (LPG) exposure, due to the fact that an electron of reducing gas was injected to p-type material resulting in increased resistance of the sensor [50]. This could explain the sensing behavior of as-grown CNTs and α-Fe_2O_3/CNTs composite based on LPG sensor. Figure 5(c) clearly depicts that the sensing behavior of CNTs without α-Fe_2O_3 is of p-type.

Figure 5(d) presents the sensor response, and α-Fe_2O_3/CNT films showed the maximum in response along with fast response/recovery time, while as-grown CNT and purified CNT films had a low response. This was due to the fact that high bonding energy among LPG atoms allows limited electron transfer from LPG molecules to the CNTs [51]. However, the purified CNTs had a quick response/recovery time because of the highly purified CNTs than that of CNT films. These results indicated that the α-Fe_2O_3/CNT films had an excellent responsive to detect the LPG.

Moreover, we observed that the time response of α-Fe_2O_3/CNTs was faster than that of as-grown CNTs. This observation can be explained by the different sensing mechanism. For as-grown CNT films, the response is attributed to the adsorption between the LPG and the surface of the carbon nanotube. On the other hand, the fast response of α-Fe_2O_3/CNT films might be due to the sensing process of the interface between the CNTs and the α-Fe_2O_3. According to this mechanism, the quick response of Fe_2O_3/CNT-based sensors could be attributed the Schottky barrier formed at α-Fe_2O_3 and CNTs junction [52]. Moreover, the annealing in air could improve the response time of α-Fe_2O_3/CNT films [53].

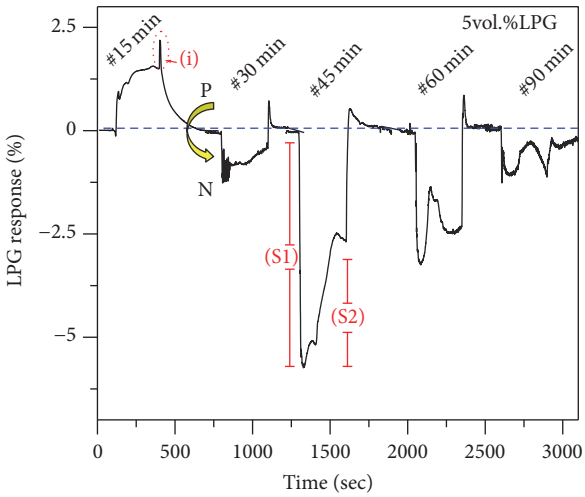

FIGURE 6: Sensing performances of α-Fe_2O_3/CNT films prepared under varying the deposition time of 15, 30, 45, 60, and 90 min.

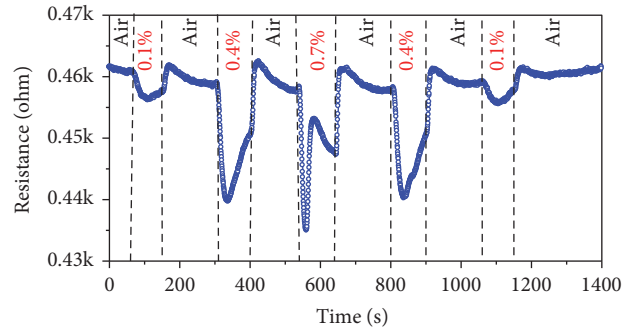

FIGURE 7: Dynamic responses of α-Fe_2O_3/CNT composite films to LPG concentrations varying from 0.1 to 0.7 vol.% in a different mix environment of air.

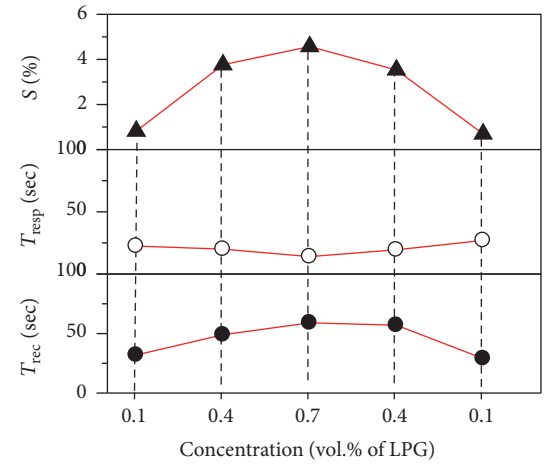

FIGURE 8: Summarizing the sensing properties of α-Fe_2O_3/CNT composite films to LPG concentrations varying from 0.1 to 0.7 vol.% in a different mix environment of air.

In next section, we investigated the effect of the deposition time on LPG sensing, as showed in Figure 6. "S1" and "S2" are defined as the sensor response of n- and p-type, respectively. The α-Fe_2O_3/CNT films were prepared under varying deposition time of 15, 30, 45, 60, and 90 min. For the sensing behavior of α-Fe_2O_3/CNT films, we found that the α-Fe_2O_3/CNT films present the both of n- and p-type behavior. However, notable behaviors of the sensor were attributed to the deposition time. α-Fe_2O_3/CNTs prepared for 15 min showed the p-type sensing behavior while α-Fe_2O_3/CNTs prepared under deposition time of 30, 45, 60, and 90 min presented n-type sensing behavior. Note that the resistance of the α-Fe_2O_3/CNT composites prepared under the deposition time of 120 min was also investigated, because of its extremely high resistance at room temperatures, which is out of the range of our instrument. Moreover, SEM and AFM images of α-Fe_2O_3/CNT films indicated that the choosing a suitable deposition time could be generated the α-Fe_2O_3/CNT films along with a highly porous structure and high roughness. This could explain the α-Fe_2O_3/CNT films prepared under deposition time of 45 min, which is the maximum response of ~6% to 5 vol.% of LPG.

To examine the sensor's multiple-cycle sensing performance under air environment, the α-Fe_2O_3/CNT films were measured under at various concentrations of 0.1, 0.4, and 0.7 vol.% of LPG diluted in zero air, as shown in Figure 7. The electrical resistance of sensors decreased upon LPG exposure and increased after replacing LPG with zero air. The sensor response, response, and recovery times of α-Fe_2O_3/CNTs on Figure 7 are summarized in Figure 8. It is observed that the sensor response and response/recovery times were stable and nearly equal at each concentration, indicating a good reproducibility of the sensing performance. Moreover, the α-Fe_2O_3/CNT films could detect LPG at concentration levels of less than 0.5 vol.% of LPG, which corresponds to 25% LEL of LPG. Note that LEL (lower explosive limit) is defined as the minimum level of concentration of LPG contained in the air sufficient enough to propagate a flame when exposed to a source of ignition.

3.5. LPG Sensing Mechanism. The sensing mechanism of the reducing gas (electron donors) like LPG results from the chemical reaction (between LPG molecules and the surface of materials) and relates to change in electrical properties of the samples, as discussed in many reports [48, 54]. For example, LPG sensing of the n-Fe_2O_3 semiconductor has been shown to be n-type sensing behaviors due to reducing in resistance when exposed to LPG [18]. In air, oxygen molecules in the ambient air absorb continuously on the empty absorption sites Fe_2O_3, which can be described by the following equations:

$$O_2\,(\text{gas}) \longleftrightarrow O_2\,(\text{adsorbed; ads}) \quad (1)$$

$$O_2\,(\text{ads}) + e^- \longleftrightarrow O_2{}^-\,(\text{ads}) \quad (2)$$

$$2C_nH_{2n+2} + 2O_2{}^- \longleftrightarrow 2H_2O + 2C_nH_{2n}O + 2e^- \quad (3)$$

Table 1: Nanocomposite materials-based LPG sensors operating at room temperature.

Years [ref.]	Materials	LPG (vol.%)	S (%)	$T_{resp.}$ /$T_{rec.}$@90%
2011 [1]	Ferric oxide	2.0	5100.0	~120 s/~150 s
2013 [4]	Ppy/TiO_2	0.10	55.0	~112 s/~130 s
2013 [11]	PTh/SnO_2 hybrid	0.5–2.5	~9.5–56.2	196–94 s/182–466 s
2014 [42]	CuO-SnO_2	0.5	~4200.0	~180 s/~200 s
2014 [10]	PANI/γ-Fe_2O_3	0.02	~140	~60 s/N/A
2014 [43]	$ZnFe_2O_4$	5.0	~1600.0	~120 s/~150 s
2014 [44]	Cu_2ZnSnS_4	0.12	~20.0	~70 s/~40 s
2016 [45]	Cu_2ZnSnS_4	0.1	~60.0	~40 s/~40 s
2017 [46]	$BaTiO_3$	0.5	50	~30 s/~60 s
This study	As-grown CNTs	5.0	~0.25	~290 s/N/A
	Purified CNTs	5.0	~0.25	~20 s/45 s
	α-Fe_2O_3/CNTs	0.1–5.0	~1.0–6.0	~25–13 s/~30–80 s

According to (1)–(3), the oxygen extracts electrons from the conduction band of Fe_2O_3 to form O_2^- (at room temperature), leading to an increase in resistance [25]. When Fe_2O_3 is exposed to LPG (C_nH_{2n+2}), O_2^- on the film surface interacts with the LPG molecules and produces gas intermediates (C_nH_{2n} : O), water (H_2O) vapor, and electron. An electron in (3) led to a decrease in resistance of Fe_2O_3 materials. In contrast, p-CNTs presented the resistance reduced upon exposure to LPG, showing p-type sensing behaviors, as illustrated in sensor response of as-grown CNTs (see in Figure 5).

Moreover, all α-Fe_2O_3/CNT films exhibited excessive recovery (point "i" in Figure 6), which is similar to that reported by Dai et al. in a gas sensor made of monolayer α-Fe_2O_3 [55]. They explained the excessive recovery due to the one-electron response, one initial electron recovery, and two-electron eventual recovery. In our work, the one-electron response has received from the LPG molecules; the two-electron recovery might be received from the oxygen/substance intermediates gas ($C_nH_{2n}O$) which may be due to the high active site on α-Fe_2O_3.

The advantageous properties of the CNTs-based gas sensor are high sensitivity and fast response; however, the CNTs-based LPG sensor is slow to respond and slow to recover. This was due to the fact that high bonding energy among LPG atoms allows limited electron transfer from LPG molecules to the CNTs [51]. In our experiment, the α-Fe_2O_3/CNTs-based LPG sensor's improved response was achieved by converting Fe, which served as catalyst for the growth of CNTs, to α-Fe_2O_3, causing an increase in LPG active sites in the CNTs. In addition, the porous morphology and the new characteristics of the nanocomposite materials such as n-Fe_2O_3/p-CNT nanocomposites make it possible to improve LPG sensing performance. Further investigations are required to clarify this kind of sensing mechanism, which will be undertaken in our future work. Moreover, our literature review shows that various materials have been used in LPG sensor applications intended for room temperature use, as shown in Table 1. Our α-Fe_2O_3/CNT films-based LPG sensors exhibited a fast response/recovery time, indicating the promise of possible applications in LPG leak detection at room temperature.

4. Conclusions

A simple fabrication of liquid petroleum gas sensor based on α-Fe_2O_3/CNT nanocomposite films is reported. α-Fe_2O_3/CNT films were successfully synthesized through the vertical floating catalyst chemical vapor deposition method (FC-CVD) using ferrocene-ethanol mist. To fabricate a sensor, the metallic Fe particles on CNTs were changed into α-Fe_2O_3 by annealing in air at 350°C. Raman spectroscopy, XPS analysis, SEM, and AFM images reveal the Fe_2O_3/CNT structure with porous and roughness structure. The sensing performance of the sensor was tested at room temperature. The sensing performance of α-Fe_2O_3/CNTs showed that it could detect LPG concentration at lower value than 25% of LEL with response/recovery time of less than 30 seconds at room temperature. These results suggest that the α-Fe_2O_3/CNTs films are a challenging material for monitoring LPG operating at room temperature.

Conflicts of Interest

The authors declare that there are no conflicts of interest regarding the publication of this paper.

Acknowledgments

The authors are grateful to the Western Digital (Thailand) for the Raman measurements. The work has been supported, in part, by the King Mongkut's Institute of Technology Ladkrabang (KMITL) Research Fund. B. Chaitongrat gratefully acknowledges the financial support for this work provided by the Higher Education Research Promotion and National Research University Project of Thailand, Office of the Higher Education Commission.

Supplementary Materials

Figure S1: (a) TEM images which represent iron nanoparticles (Fe NPs) at surface of the growth of CNTs; (b) particle-size distribution of the Fe NPs performed by measuring 45

individual NPs on the TEM images. Figure S1(a) shows the TEM image of the as-grown CNT films, which consisted of the randomly oriented entangled CNTs. The small-diameter CNTs were coated with Fe NPs, and some of these CNTs were coated with Fe NP clusters. These NPs were metallic iron (using XPS). An estimation of the distribution of Fe NPs' sizes performed by measuring each NP obtained from TEM images yielded an average particle size of ~7.33 nm, as shown in Figure 1S(b). *(Supplementary Materials)*

References

[1] B. C. Yadav, S. Singh, and A. Yadav, "Nanonails structured ferric oxide thick film as room temperature liquefied petroleum gas (LPG) sensor," *Applied Surface Science*, vol. 257, no. 6, pp. 1960–1966, 2011.

[2] B. Thomas and B. Skariah, "Spray deposited Mg-doped SnO2 thin film LPG sensor: XPS and EDX analysis in relation to deposition temperature and doping," *Journal of Alloys and Compounds*, vol. 625, pp. 231–240, 2015.

[3] F. Pourfayaz, A. Khodadadi, Y. Mortazavi, and S. S. Mohajerzadeh, "CeO_2 doped SnO_2 sensor selective to ethanol in presence of CO, LPG and CH4," *Sensors and Actuators B: Chemical*, vol. 108, no. 1-2, pp. 172–176, 2005.

[4] R. N. Bulakhe, S. V. Patil, P. R. Deshmukh, N. M. Shinde, and C. D. Lokhande, "Fabrication and performance of polypyrrole (Ppy)/TiO2 heterojunction for room temperature operated LPG sensor," *Sensors and Actuators B: Chemical*, vol. 181, pp. 417–423, 2013.

[5] V. Talwar, O. Singh, and R. C. Singh, "ZnO assisted polyaniline nanofibers and its application as ammonia gas sensor," *Sensors and Actuators B: Chemical*, vol. 191, pp. 276–282, 2014.

[6] S. Singh, A. Singh, M. Wan et al., "Fabrication of self-assembled hierarchical flowerlike zinc stannate thin film and its application as liquefied petroleum gas sensor," *Sensors and Actuators B: Chemical*, vol. 205, pp. 102–110, 2014.

[7] S. Singh, V. Gupta, B. C. Yadav, P. Tandon, and A. K. Singh, "Structural analysis of nanostructured iron antimonate by experimental and quantum chemical simulation and its LPG sensing," *Sensors and Actuators B: Chemical*, vol. 195, pp. 373–381, 2014.

[8] D. Haridas, A. Chowdhuri, K. Sreenivas, and V. Gupta, "Enhanced room temperature response of SnO2 thin film sensor loaded with Pt catalyst clusters under UV radiation for LPG," *Sensors and Actuators B: Chemical*, vol. 153, no. 1, pp. 152–157, 2011.

[9] D. S. Dhawale, R. R. Salunkhe, U. M. Patil, K. V. Gurav, A. M. More, and C. D. Lokhande, "Room temperature liquefied petroleum gas (LPG) sensor based on p-polyaniline/n-TiO2 heterojunction," *Sensors and Actuators B: Chemical*, vol. 134, no. 2, pp. 988–992, 2008.

[10] T. Sen, N. G. Shimpi, S. Mishra, and R. Sharma, "Polyaniline/γ-Fe2O3 nanocomposite for room temperature LPG sensing," *Sensors and Actuators B: Chemical*, vol. 190, pp. 120–126, 2014.

[11] S. S. Barkade, D. V. Pinjari, U. T. Nakate et al., "Ultrasound assisted synthesis of polythiophene/SnO2 hybrid nanolatex particles for LPG sensing," *Chemical Engineering and Processing: Process Intensification*, vol. 74, pp. 115–123, 2013.

[12] N. M. Vuong, N. D. Chinh, B. T. Huy, and Y.-I. Lee, "CuO-decorated ZnO hierarchical nanostructures as efficient and established sensing materials for H2S Gas Sensors," *Scientific Reports*, vol. 6, Article ID 26736, 2016.

[13] B.-Y. Wei et al., "A Novel SnO2 Gas Sensor Doped With Carbon Nanotubes Operating at Room Temperature," *Sensors and Actuators B: Chemical*, vol. 101, no. 1, pp. 81–89, 2004.

[14] C. Bittencourt, A. Felten, E. H. Espinosa et al., "WO_3 films modified with functionalised multi-wall carbon nanotubes: morphological, compositional and gas response studies," *Sensors and Actuators B: Chemical*, vol. 115, no. 1, pp. 33–41, 2006.

[15] S. Liang, H. Bi, J. Ding, J. Zhu, Q. Han, and X. Wang, "Synthesis of α-Fe2O3 with the aid of graphene and its gas-sensing property to ethanol," *Ceramics International*, vol. 41, no. 5, pp. 6978–6984, 2015.

[16] M. Tadic, N. Citakovic, M. Panjan et al., "Synthesis, morphology and microstructure of pomegranate-like hematite (α-Fe 2O 3) superstructure with high coercivity," *Journal of Alloys and Compounds*, vol. 543, pp. 118–124, 2012.

[17] N. D. Cuong, D. Q. Khieu, T. T. Hoa et al., "Facile synthesis of α-Fe2O3 nanoparticles for high-performance CO gas sensor," *Materials Research Bulletin*, vol. 68, pp. 302–307, 2015.

[18] D. Patil, V. Patil, and P. Patil, "Highly sensitive and selective LPG sensor based on α-Fe 2O3 nanorods," *Sensors and Actuators B: Chemical*, vol. 152, no. 2, pp. 299–306, 2011.

[19] Q. Tan, J. Fang, W. Liu, J. Xiong, and W. Zhang, "Acetone sensing properties of a gas sensor composed of carbon nanotubes doped with iron oxide nanopowder," *Sensors*, vol. 15, no. 11, pp. 28502–28512, 2015.

[20] R. E. Smalley et al., *Carbon Nanotubes: Synthesis, Structure, Properties, And Applications*, vol. 80, Springer Science and Business Media, Berlin, Germany, 2003.

[21] S. Chaisitsak, B. Chaithongrat, J. Nukeaw, and A. Tuantranont, "Organic vaporensors based on single-walled CNTs," in *Proceedings of the 2006 5th IEEE Conference on Sensors*, pp. 1081–1084, Republic of Korea, October 2006.

[22] J. Kong, N. R. Franklin, C. Zhou et al., "Nanotube molecular wires as chemical sensors," *Science*, vol. 287, no. 5453, pp. 622–625, 2000.

[23] L. Valentini, I. Armentano, J. M. Kenny, C. Cantalini, L. Lozzi, and S. Santucci, "Sensors for sub-ppm NO2 gas detection based on carbon nanotube thin films," *Applied Physics Letters*, vol. 82, no. 6, pp. 961–963, 2003.

[24] J. Chuen, "Effects of the Growth Time and the Thickness of the Buffer Layer on the Quality of the Carbon Nanotubes," *Journal of Nanomaterials*, vol. 2017, 6 pages, 2017.

[25] P. Muthukumaran, C. Sumathi, J. Wilson, C. Sekar, S. G. Leonardi, and G. Neri, "Fe2O3/Carbon nanotube-based resistive sensors for the selective ammonia gas sensing," *Sensor Letters*, vol. 12, no. 1, pp. 17–23, 2014.

[26] D. Jung, M. Han, and G. S. Lee, "Room-temperature gas sensor using carbon nanotube with cobalt oxides," *Sensors and Actuators B: Chemical*, vol. 204, pp. 596–601, 2014.

[27] M. Tavakkoli, T. Kallio, O. Reynaud et al., "Maghemite nanoparticles decorated on carbon nanotubes as efficient electrocatalysts for the oxygen evolution reaction," *Journal of Materials Chemistry A*, vol. 4, no. 14, pp. 5216–5222, 2016.

[28] K. Jantharamatsakarn and S. Chaisitsak, "Ferrocene-ethanol-mist CVD grown SWCNT films as transparent electrodes," in *Proceedings of the 7th International Conference on Materials for Advanced Technologies, ICMAT 2013, Symposium G on Carbon Nanotubes and Graphene: Synthesis, Functionalisation and Applications*, pp. 49–58, Singapore, July 2013.

[29] M. S. Dresselhaus, G. Dresselhaus, R. Saito, and A. Jorio, "Raman spectroscopy of carbon nanotubes," *Physics Reports*, vol. 409, no. 2, pp. 47–99, 2005.

[30] S. Nagasawa, M. Yudasaka, K. Hirahara, T. Ichihashi, and S. Iijima, "Effect of oxidation on single-wall carbon nanotubes," *Chemical Physics Letters*, vol. 328, no. 4-6, pp. 374–380, 2000.

[31] M. Lübbe, A. M. Gigler, R. W. Stark, and W. Moritz, "Identification of iron oxide phases in thin films grown on Al2O3(0 0 0 1) by Raman spectroscopy and X-ray diffraction," *Surface Science*, vol. 604, no. 7-8, pp. 679–685, 2010.

[32] V. Balouria, A. Kumar, S. Samanta et al., "Nano-crystalline Fe2O3 thin films for ppm level detection of H2S," *Sensors and Actuators B: Chemical*, vol. 181, pp. 471–478, 2013.

[33] T. J. Simmons, N. Maeda, J. Miao, M. Bravo-Sanchez, J. S. Dordick, and R. J. Linhardt, "Self-assembly of carbon nanotube films from room temperature ionic liquids," *Carbon*, vol. 58, pp. 226–231, 2013.

[34] O. Akhavan and E. Ghaderi, "Self-accumulated Ag nanoparticles on mesoporous TiO_2 thin film with high bactericidal activities," *Surface and Coatings Technology*, vol. 204, no. 21-22, pp. 3676–3683, 2010.

[35] N. A. Zubir, C. Yacou, J. Motuzas, X. Zhang, and J. C. Diniz Da Costa, "Structural and functional investigation of graphene oxide-Fe 3 O 4 nanocomposites for the heterogeneous Fenton-like reaction," *Scientific Reports*, vol. 4, Article ID 04594, 2014.

[36] F. L. Souza, K. P. Lopes, P. A. P. Nascente, and E. R. Leite, "Nanostructured hematite thin films produced by spin-coating deposition solution: application in water splitting," *Solar Energy Materials & Solar Cells*, vol. 93, no. 3, pp. 362–368, 2009.

[37] E. F. Antunes, V. G. De Resende, U. A. Mengui, J. B. M. Cunha, E. J. Corat, and M. Massi, "Analyses of residual iron in carbon nanotubes produced by camphor/ferrocene pyrolysis and purified by high temperature annealing," *Applied Surface Science*, vol. 257, no. 18, pp. 8038–8043, 2011.

[38] A. Furlan, U. Jansson, J. Lu, L. Hultman, and M. Magnuson, "Structure and bonding in amorphous iron carbide thin films," *Journal of Physics: Condensed Matter*, vol. 27, no. 4, Article ID 045002, 2015.

[39] M. T. Martínez, M. A. Callejas, A. M. Benito et al., "Sensitivity of single wall carbon nanotubes to oxidative processing: Structural modification, intercalation and functionalisation," *Carbon*, vol. 41, no. 12, pp. 2247–2256, 2003.

[40] L. Stobinski, B. Lesiak, L. Kövér et al., "Multiwall carbon nanotubes purification and oxidation by nitric acid studied by the FTIR and electron spectroscopy methods," *Journal of Alloys and Compounds*, vol. 501, no. 1, pp. 77–84, 2010.

[41] A. Benko, A. Przekora, A. Wesełucha-Birczyńska, M. Nocuń, G. Ginalska, and M. Błażewicz, "Fabrication of multi-walled carbon nanotube layers with selected properties via electrophoretic deposition: physicochemical and biological characterization," *Applied Physics A: Materials Science & Processing*, vol. 122, no. 4, article no. 447, 2016.

[42] S. Singh, N. Verma, A. Singh, and B. C. Yadav, "Synthesis and characterization of CuO-SnO2 nanocomposite and its application as liquefied petroleum gas sensor," *Materials Science in Semiconductor Processing*, vol. 18, no. 1, pp. 88–96, 2014.

[43] R. Srivastava and B. Yadav, "Nanostructured ZnFe2O4 thick film as room temperature liquefied petroleum gas sensor," *Journal of Experimental Nanoscience*, vol. 10, no. 9, pp. 703–717, 2014.

[44] K. V. Gurav, S. W. Shin, U. M. Patil et al., "Cu2ZnSnS4 (CZTS)-based room temperature liquefied petroleum gas (LPG) sensor," *Sensors and Actuators B: Chemical*, vol. 190, pp. 408–413, 2014.

[45] S. J. Patil, R. N. Bulakhe, and C. D. Lokhande, "Liquefied petroleum gas (LPG) sensing using spray deposited Cu2ZnSnS4 thin film," *Journal of Analytical and Applied Pyrolysis*, vol. 117, pp. 310–316, 2016.

[46] M. Singh, B. C. Yadav, A. Ranjan, M. Kaur, and S. K. Gupta, "Synthesis and characterization of perovskite barium titanate thin film and its application as LPG sensor," *Sensors and Actuators B: Chemical*, vol. 241, pp. 1170–1178, 2017.

[47] S. Chaisitsak, "Nanocrystalline SnO_2:F thin films for liquid petroleum gas sensors," *Sensors*, vol. 11, no. 7, pp. 7127–7140, 2011.

[48] V. V. Jadhav, S. A. Patil, D. V. Shinde et al., "Hematite nanostructures: Morphology-mediated liquefied petroleum gas sensors," *Sensors and Actuators B: Chemical*, vol. 188, pp. 669–674, 2013.

[49] V. N. Mishra and R. P. Agarwal, "Sensitivity, response and recovery time of SnO2 based thick-film sensor array for H2, CO, CH4 and LPG," *Microelectronics Journal*, vol. 29, no. 11, pp. 861–874, 1998.

[50] R. K. Roy, M. P. Chowdhury, and A. K. Pal, "Room temperature sensor based on carbon nanotubes and nanofibres for methane detection," *Vacuum*, vol. 77, no. 3, pp. 223–229, 2005.

[51] M. D. Ganji, A. Mirnejad, and A. Najafi, "Theoretical investigation of methane adsorption onto boron nitride and carbon nanotubes," *Science and Technology of Advanced Materials*, vol. 11, no. 4, Article ID 045001, 2010.

[52] J. Suehiro, H. Imakiire, S.-I. Hidaka et al., "Schottky-type response of carbon nanotube NO 2 gas sensor fabricated onto aluminum electrodes by dielectrophoresis," *Sensors and Actuators B: Chemical*, vol. 114, no. 2, pp. 943–949, 2006.

[53] S. Mao, S. Cui, K. Yu, Z. Wen, G. Lu, and J. Chen, "Ultrafast hydrogen sensing through hybrids of semiconducting single-walled carbon nanotubes and tin oxide nanocrystals," *Nanoscale*, vol. 4, no. 4, pp. 1275–1279, 2012.

[54] L. A. Patil, M. D. Shinde, A. R. Bari, V. V. Deo, D. M. Patil, and M. P. Kaushik, "Fe_2O_3 modified thick films of nanostructured SnO_2 powder consisting of hollow microspheres synthesized from pyrolysis of ultrasonically atomized aerosol for LPG sensing," *Sensors and Actuators B: Chemical*, vol. 155, no. 1, pp. 174–182, 2011.

[55] Z. Dai, C.-S. Lee, Y. Tian, I.-D. Kim, and J.-H. Lee, "Highly reversible switching from P- to N-type NO2 sensing in a monolayer Fe2O3 inverse opal film and the associated P-N transition phase diagram," *Journal of Materials Chemistry A*, vol. 3, no. 7, pp. 3372–3381, 2015.